Article

Design and Synthesis of a Ratiometric Photoacoustic Probe for in situ Imaging of Zinc Ions in Deep-Tissue in vivo

Chaobang Zhang, Rongkang Gao, Liangliang Zhang, Chengbo Liu, Zhengmin Yang, and Shulin Zhao

Anal. Chem., **Just Accepted Manuscript** • DOI: 10.1021/acs.analchem.9b05431 • Publication Date (Web): 10 Mar 2020

Design and Synthesis of a Ratiometric Photoacoustic Probe for *in situ* Imaging of Zinc Ions in Deep-Tissue *in vivo*

Authors: Chaobang Zhang,[†,#] Rongkang Gao,[‡,#] Liangliang Zhang,[†] Chengbo Liu,[*,‡] Zhengmin Yang,[†] and Shulin Zhao[*,†]

Affiliation: [†] State Key Laboratory for the Chemistry and Molecular Engineering of Medicinal Resources, Guangxi Normal University, Guilin, 541004, China

[‡] Research Laboratory for Biomedical Optics and Molecular Imaging, CAS Key Laboratory of Health Informatics, Shenzhen Institutes of Advanced Technology, Chinese Academy of Sciences, Shenzhen 518055, China.

Corresponding author: Professor Shulin Zhao and Chengbo Liu

E-mail: zhaoshulin001@163.com

cb.liu@siat.ac.cn

ABSTRACT: As a non-invasive deep tissue imaging technique, photoacoustic (PA) imaging has great application potential in biomedicine and molecular diagnosis. Zinc ion (Zn^{2+}), a necessary metal ion in human body, plays a very important role in the regulation of gene transcription and metalloenzyme function. The imbalance of Zn^{2+} homeostasis is also associated with a variety of neurological diseases. Therefore, it is critically important to accurately image the steady state changes of Zn^{2+} *in vivo*. However, no PA imaging method is currently available for Zn^{2+}. To this end, we designed and synthesized the first PA probe of Zn^{2+} namely CR-1 for *in situ* ratiometric imaging of Zn^{2+} in deep-tissue *in vivo*. The CR-1 combined with Zn^{2+} weakened the conjugation system of the π electron in the CR-1 molecule, which resulted in the blue shift of its absorption peak from 710 nm to 532 nm. The PA signal intensity decreased at 710 nm and increased at 532 nm, and the ratiometric PA signal at these two wavelengths (PA_{532}/PA_{710}) showed a good linear relationship with the concentration of Zn^{2+} in the range of 0 to 50 μM, with a detection limit as low as 170 nM. Furthermore, this probe exhibits extremely fast responsiveness, highly selective and excellent biocompatibility. We have used the developed PA probe for the ratiometric PA imaging of Zn^{2+} in thigh tissue of mice, and still can image accurately Zn^{2+} after covering a chicken breast tissue on the surface of mice thigh. In light of these outstanding features, the developed PA probe has high potential for imaging Zn^{2+} in deep tissues, thus it will open up new avenues for the study of the complex biochemical processes involving Zn^{2+} *in vivo*.

Zinc ion (Zn^{2+}), a necessary metal ion in human body, plays a very important role in the regulation of the function of metalloenzymes, and gene transcription of many proteins involved in a variety of cellular functions.[1,2] The imbalance of Zn^{2+} homeostasis can leads to a variety of nervous system diseases.[3,4] In addition, change in Zn^{2+} concentration in the human body has been found to be closely associated with the development of prostate cancer.[5] Therefore, it is crucial to accurately image the changes of Zn^{2+} *in vivo*.

The traditional methods for the imaging of Zn^{2+} are mass spectrometry (MS) imaging, magnetic resonance imaging (MRI) and photoluminescence (PL) imaging.[6-8] Besides providing only general information on the total amount of Zn^{2+} and requiring sample pretreatment, the MS technique cannot be used to image Zn^{2+} in the body in real time. MRI can non-invasively image Zn^{2+} in real-time, but it is limited by lower sensitivity and resolution. PL imaging has the advantages of high sensitivity and resolution, but due to the strong scattering of light in biological tissues, its imaging depth is only about 1 mm, and thus, its application *in vivo* is limited. The recently developed photoacoustic (PA) imaging technique is a novel technology that combines the high contrast of optical imaging with the high resolution and deep-tissue penetration of ultrasonic imaging.[9-11] Since the attenuation of sound waves in biological tissues is three orders of magnitude lower than that of photons, PA imaging can be used to perform real-time non-invasive high-resolution deep-tissue imaging. Therefore, the PA imaging technique has great application potential in biomedicine and molecular diagnosis.

The PA imaging technology can achieve adequate resolution and image contrast at a certain depth and provide morphological and functional information. Accordingly, it has received increasing research interest in the field of biomolecule imaging. In the past few years, PA imaging probes for various analytes have been developed and used for imaging of biological small molecules,[12,13] tumor tissue,[14-16] tumor-associated protease,[17] calcium ion,[18,19] copper ion[20] and hypochlorous acid.[21] These probes have the potential to play an important role in biomedical research and early diagnosis of target diseases. However, to the best of our knowledge, no PA imaging probe for Zn^{2+} imaging has been reported.

Ratiometric PA imaging, through its built-in self-calibration system, can eliminate the interference from the internal environment, such as uneven probe accumulation and unstable excitation light intensity.[22] Thus, the ratiometric PA imaging has preferable application prospect for reliable imaging of biological tissue *in vivo*. In this study, we designed and synthesized a ratiometric PA imaging probe of Zn^{2+}, namely CR-1, for highly selective ratiometric imaging of Zn^{2+} *in vivo* deep-tissue. The complexation of CR-1 with Zn^{2+} resulted in the blue shift of its absorption peak from 710 nm to 532 nm. The PA signal intensity decreased at 710 nm and increased at 532 nm, and the ratiometric PA signal at these two wavelengths (PA_{532}/PA_{710}) exhibited a good linear relationship with the concentration of Zn^{2+}, while other ions have no influence. We have demonstrated that the biological application of the CR-1 by reversible ratiometric PA imaging of Zn^{2+} in the thigh tissue of mice.

EXPERIMENTAL SECTION

Reagents and Materials. N,N-Dimethylformamide (DMF), phthalimide potassium salt, 2,6-bis(chloromethyl)pyridine and di(2-picolyl)amine were purchased from Accustandard Inc. (J&K Scientific Ltd., Beijing, China). Hydrazine monohydrate, N,N,N′,N′-tetrakis (2-pyridylmethyl)ethylenediamine (TPEN), nitrilotriacetic acid and indocyanine green (ICG) were obtained from Sigma-Aldrich Co. (St. Louis, MO, USA) and used without any further purification. Milli-Q water with a resistivity above 18 MΩ·cm was used in the experiments.

Apparatus. Proton (^{1}H) or ^{13}C nuclear magnetic resonance (NMR) spectroscopy was performed on a Bruker Avance III HD 400 MHz NMR spectrometer (Bruker BioSpin GmbH, Ettlingen, Germany). MS analysis was performed on an Exactive Liquid Chromatography-Mass Spectrometry (LC-MS) system (Thermo Fisher Scientific Inc., Waltham, MA, USA). UV-vis absorption spectra were performed on a Cary 60 UV-vis spectrophotometer (Agilent Technologies Inc., Santa Clara, CA, USA). Cytotoxicity tests were performed using a Multiskan MK3 Enzyme Mark spectrophotometer (Thermo Fisher Scientific Inc.). A homemade PA computed tomography system was used in all PA imaging experiments.[23]

Synthesis of CR-1. The heptamethyl-carboline derivative (IR825, 0.38 mmol) and tris (2-pyridylmethyl) amine (TMPA, 0.40 mmol) were added into a 100-mL round bottom flask under nitrogen protection. Finally, 15 mL of DMF was added into the round bottom flask, the mixed solution was heated to 70 °C with continuous

stirring and refluxed for 1 h. Subsequently, the solvent was removed by vacuum distillation. The crude product was then purified by column chromatography using DCM/MeOH (v/v, 20:1) as eluent to produce a blue solid product, namely CR-1, with a yield of 31.3%. [M+H]+=894.520 (calcd. for $C_{61}H_{64}N_7^+$: 894.521). ^{1}H NMR (400 MHz, CD_2Cl_2) δ=8.39 (d, J=4.9 Hz, 2H), 7.93 (d, J=8.5 Hz, 2H), 7.82–7.79 (m, 3H), 7.78 (d, J=2.3 Hz, 2H), 7.72 (d, J=7.7 Hz, 1H), 7.60 (td, J=7.5, 1.8 Hz, 3H), 7.54 (d, J=7.8 Hz, 2H), 7.46–7.41 (m, 2H), 7.40 (d, J=8.7 Hz, 2H), 7.32–7.29 (m, 2H), 7.28 (d, J=0.8 Hz, 1H), 7.22 (d, J=7.9 Hz, 1H), 7.18 (d, J=8.8 Hz, 2H), 7.08–7.06 (m, 1H), 7.05 (d, J=2.4 Hz, 1H), 5.68 (d, J=13.1 Hz, 2H), 4.02 (s, 2H), 3.94 (d, J=10.9 Hz, 6H), 2.51 (t, J=6.2 Hz, 4H), 2.17 (t, J=7.6 Hz, 2H), 1.92 (dd, J=10.5, 4.2 Hz, 2H), 1.81–1.77 (m, 2H), 1.74 (s, 12H), 1.53–1.39 (m, 4H). ^{13}C NMR (100 MHz, CD_2Cl_2) δ=176.41, 169.14, 168.17, 157.97, 155.46, 149.21, 148.51, 148.33, 147.72, 147.66, 147.50, 145.86, 140.17, 139.42, 139.06, 138.78, 138.69, 138.24, 137.84, 137.51, 137.31, 131.60, 131.10, 130.23, 129.99, 128.60, 127.47, 127.30, 127.19, 124.84, 124.65, 124.05, 123.94, 123.66, 122.88, 122.73, 122.49, 121.99, 120.83, 120.53, 119.06, 118.99, 118.81, 113.92, 109.98, 94.35, 60.07, 59.71, 49.75, 34.94, 34.56, 32.04, 31.27, 30.09, 29.81, 29.48, 28.07, 22.81, 14.02, 11.82.

Determination of apparent dissociation constant of CR-1- Zn^{2+} complex. The absorption spectra **of** CR-1-Zn^{2+} complex solutions were used to determine the apparent dissociation constant (K_d),[24] and the following equation is used to calculate the K_d: $R=(R_{max}[Zn^{2+}]+K_d R_{min})/(K_d+[Zn^{2+}])$. In the above formula, R is the absorption ratio (Abs_{532}/Abs_{710}), R_{max} is the maximum absorption ratio, R_{min} is the absorption

ratio without adding Zn^{2+}, and [Zn^{2+}] is the free concentration of Zn^{2+}. 10 mM nitrilotriacetic acid was used to regulate the concentration of free Zn^{2+}.

In Vitro Cytotoxicity Test and *in Vivo* Toxicity Assessment. The human prostate carcinoma 22Rv1 cell line was selected as model cells, and the MTT (methylthiazoly-ldiphenyl-tetrazolium bromide) assay was used to evaluate the cytotoxicity of CR-1. The 22Rv1cells were incubated on 96-well cell culture plates and incubated for 24 h at 37 °C with 5% CO_2. Then, different concentrations of CR-1 (0, 5, 10, 25, 50, 100 μM) were added to the cells in the wells of the culture plate, and incubated for another 24 h. Subsequently, 15 μL of MTT solution (5 mg/mL) was added to each well, and the cells in plate was further incubated for an additional 4 h. Afterwards, the cell culture medium was removed from the wells and 150 μL of DMSO was added into each well. The absorbance of the solution in each well was measured using a Multiskan MK3 Enzyme Mark spectrophotometer at a wavelength of 570 nm. The *in vivo* toxicity of CR-1 was evaluated in female BALB/c mice (20-22 g) by monitoring the body weight of the mice every day for 14 days, after intravenous injection into the tail vein of the mice of phosphate-buffered saline (PBS) for the control group and CR-1 (3 mg/kg) for the experimental group.

Animal. The 8-week old female BALB/c mice were supplied by Hunan SJA Laboratory Animal Co., Ltd. (Changsha, China). Animal handling procedures were approved by the Animal Ethics Committee of Guangxi Normal University (No. 20150325-XC). During the weight monitoring experiment, the weight of the mice and any sign of clinical abnormality were recorded daily. Once a mouse was determined

to be unable to eat, injured or dead, the mouse was excluded from the study.

***In Vivo* PA Imaging.** Fifteen female BALB/c mice were divided into 5 groups (3 mice in each group). All the solutions were injected subcutaneously into the thighs of the mouse under the guidance of ultrasound imaging. The first group (control group) received 50 μL HEPES buffer; the second group received 50 μL CR-1 solution (50 μM); the third group received a subcutaneous injection of a Zn^{2+} solution (0.25 mg/kg), followed by 50 μL of CR-1 solution (50 μM); the fourth group received a subcutaneous injection of a Zn^{2+} solution (0.5 mg/kg), followed by 50 μL of CR-1 solution (50 μM); the fifth group received a subcutaneous injected of a mixture of Zn^{2+} (0.5 mg/kg) and the same amount of TPEN, followed by 50 μL of CR-1 solution (50 μM). The PA signals in the thigh of the mice were measured with the self-made optical coherence tomography system (PACT) using a laser at the wavelengths of 532 nm and 710 nm. To further demonstrate that CR-1 still has the ability to image Zn^{2+} *in vivo* deep tissue, subcutaneous injection of Zn^{2+} solution (0.5 mg/kg) into the thigh of mice was followed by injection of CR-1 solution (50 μM，50 μL). PA signals at 532 nm and 710 nm were then measured after covering chicken breast in the injection area.

RESULTS AND DISCUSSION

Design and Synthesis of CR-1. The synthesis route of CR-1 is shown in Figure 1. In developing a high sensitive PA imaging probe of Zn^{2+}, firstly, an Zn^{2+} ligand (TMPA) was synthesized according to the method reported by Yoon and

co-workers.[25,26] Then, a near-infrared dye molecule (IR825) was synthesized by the condensation reaction (Supporting Information). Ultimately, the target product CR-1 was obtained by the nucleophilic substitution reaction between IR825 and TMPA. Figures S1–S3 reveal the nuclear magnetic resonance (NMR) spectra and mass spectrometry (MS) spectrum of IR825. Figures S4-S6 display the NMR spectra and MS spectrum of CR-1. The synthesized CR-1 is very stable in aqueous solution (Figure S7) and has a large molar absorption coefficient (Figure S8), thus it readily yields a high photoacoustic signal.

Principle for PA Imaging of Zn^{2+}. The CR-1 consists of a heptamethyl-carboline derivative (IR825) and the Zn^{2+} ligand (TMPA). The molecular structure of this probe and the reaction mechanism with Zn^{2+} are illustrated in Scheme 1. When CR-1 interacts with Zn^{2+}, the five nitrogen atoms on the TMPA group of the probe coordinate with Zn^{2+}, thus causing the nitrogen atom attached to the IR825 molecule to remove one hydrogen atom. Subsequently, the double bonds on IR825 are rearranged, which weakens the π electron conjugated system and shifts the absorption peak of CR-1 from 710 nm to 532 nm (Scheme 1a). When the laser was used at the wavelengths of 710 nm and 532 nm, the PA_{710} signal decreased, while the PA_{532} signal increased (Scheme 1b). In addition, there is a good linear relationship between the ratio of the PA signal (PA_{532}/PA_{710}) and the concentration of Zn^{2+} in a certain concentration range, so that the PA_{532}/PA_{710} ratio-based PA imaging can be used to monitor Zn^{2+}*in vivo*.

Feasibility of CR-1 as PA Probe of Zn^{2+}. To investigate the feasibility of using

CR-1 as a PA probe for ratiometric PA imaging of Zn^{2+}, we examined the changes in the absorption spectrum after the reaction of CR-1 with Zn^{2+}. The ultraviolet-visible (UV-vis) absorption spectra of the CR-1 solutions with different concentrations of Zn^{2+} are shown in Figure 2a. These spectra reveal that, with the increase of Zn^{2+} concentration in the range of 0-5 μM, the absorption intensity at 710 nm (Abs_{710}) of the CR-1 solutions decreases gradually, while the absorption intensity at 532 nm (Abs_{532}) increases gradually. The response process can be completed in seconds, and the color of the solution changes from light blue to pink (inset in Figure 2a). The reaction mechanism between CR-1 and Zn^{2+} at a 1:1 was confirmed by electrospray ionization-mass spectrometry (ESI-MS) (Figures S9 and S10). The m/z peak of CR-1 is located at 894.52124 (calculated value was 894.5200), and the m/z peak of CR-1 combined with Zn^{2+} is located at 478.72183 (calculated value was 478.72). The apparent dissociation constant (K_d) for CR-1 binding to Zn^{2+} was determined to be 4.3 nM by plotting the absorption ratio at 532 and 710 nm (Figure S11). Which is higher than that of di(2-picol)amine (23 nM).[27] In addition, we found a good linear relationship between the ratio of absorption intensity (Abs_{532}/Abs_{710}) of CR-1 and the concentration of Zn^{2+} in the range of 0-5 μM (Figure 2c), with a limit of detection as low as 87 nM. Subsequently, the PA signals of CR-1 produced with different concentrations of Zn^{2+} were measured *in vitro,* with the increase of Zn^{2+} concentration, the PA signals of CR-1 solution at 710 nm was gradually weakened, while that at 532 nm was gradually enhanced (Figure 2b). These results reveal that the ratiometric PA signal (PA_{532}/PA_{710}) of CR-1 has a good linear relationship with the concentration of

Zn^{2+} in the range of 0-50 μM, with a detection limit as low as 170 nM (Figure 2d). Since the gray matter region of the brain contains about 0.5 mM of Zn^{2+}.[28] Therefore, we think that such a detection limit is much lower than the content of Zn^{2+} in the brain, indicating that CR-1 has considerable potential to detect Zn^{2+} in the brain or other biological tissues by ratiometric PA imaging.

Photostability of CR-1 prob for Zn^{2+} detection. One of the biggest challenges of using cyanine dyes for photoacoustic probe development is rapid photobleaching. Therefore, we evaluated the photostability of using CR-1 as a photoacoustic probe of Zn^{2+}, the result is shown in Figure S12. Although the photostability of CR-1 is slightly worse than that of ICG, the photoacoustic signal of the probe remains stable after 50 cycles of photoacoustic imaging (Figure S13). More importantly, even though the probe suffered severe photobleaching at the detection of Zn^{2+}, the absorption ratio of the probe (Abs_{532}/Abs_{710}) did not change significantly (Figure S14). Therefore, CR-1 possesses sufficient photostability for photoacoustic imaging of Zn^{2+}.

Reversibility of Binding Reaction Between CR-1 and Zn^{2+}. The reversibility of the binding reaction between CR-1 and Zn^{2+} was studied using N, N, N', N'-tetrakis (2-pyri-dylmethyl) ethylenediamine (TPEN) as a competitive reagent. The result shown in Figure 3a reveals that after adding Zn^{2+} to CR-1 solution, the ratio of absorption intensity (Abs_{532}/Abs_{710}) rapidly increased, and then, after adding an excessive amount of TPEN, rapidly decreased to its original value. After adding excessive Zn^{2+} again, the value of Abs_{532}/Ab_{710} returned to the same level. The repeat of such operation 5 times, all show the same phenomenon. When the ratiometric PA

intensity of the solution (PA_{532}/PA_{710}) is measured, the reversible cycle process can also be observed (Figure 3b), indicating that the binding reaction between CR-1 and Zn^{2+} is reversible. In addition, we also found that at pH value between 6.2 and 8.2, the Abs_{532}/Abs_{710} and PA_{532}/PA_{710} values of CR-1 solution remained basically unchanged, while the Abs_{532}/Abs_{710} and PA_{532}/PA_{710} values of the complex increased with the increase of the pH value of the solution (Figure S15). These findings show that the CR-1 probe has good stability in the range of pH 6.2-8.2. The sensitivity of PA imaging for Zn^{2+} increases with the increase of the environmental pH value. Although the sensitivity increases with increasing pH value, the PA_{532}/PA_{710} value is about 0.36 in the presence of trace Zn^{2+} even at pH 6.2, which is still 3.2 times higher than the probe itself (about 0.11). In general, the brain maintains its pH around 7.4 by regulating acid-base balance.[29] Accordingly, the CR-1 probe can monitor Zn^{2+} levels by ratiometric PA imaging in physiological conditions (pH 7.4).

Specificity of the CR-1 for Zn^{2+}. We investigated the specificity of the CR-1 probe for Zn^{2+}, and the results are presented in Figure 4a and Figure S16a. The results reveal that the maximum absorption of the CR-1 solution shifts from 710 nm to 532 nm only in the presence of Zn^{2+}. At the same time, the PA signal of CR-1 solution at 710 nm was weakened, while that at 532 nm was enhanced. Apart from the slight interference due to Cu^{2+}, other metal ions including Ag^{+}, Fe^{2+}, Ca^{2+}, Fe^{3+}, Ni^{2+}, Cd^{2+}, Na^{+}, K^{+}, Al^{3+}, Pb^{2+}, Cr^{3+}, Mn^{2+}, Hg^{2+}, Co^{2+} and Mg^{2+} do not interfere with Zn^{2+} detection, and the ratio of PA intensity (PA_{532}/PA_{710}) and the ratio of absorption intensity (Abs_{532}/Abs_{710}) remain basically unchanged (Figure 4b, Figure S16b).

Moreover, other metal ions do not interfere with the combination of the CR-1 probe and Zn^{2+}, and the absorption intensity (Abs_{532}/Abs_{710}) and PA strength (PA_{532}/PA_{710}) ratios of the CR-1 solution at the wavelengths of 710 nm and 532 nm in the presence of Zn^{2+} with various metal ions remain essentially constant (Figure 4c and Figure S17). These results show that the CR-1 probe is a highly-specific PA probe for the detection of Zn^{2+}.

Cytotoxicity and Biocompatibility of the CR-1. We also evaluated the cytotoxicity and biocompatibility of the CR-1. First, the cytotoxicity of CR-1 was determined by the MTT assay. As shown in Figure 5a, the survival rate of 22Rv1 cells incubated with CR-1 solution for 24 h was still more than 85%. Additionally, as shown in Figure 5b, the assessment of the biocompatibility of CR-1 in mice by tail vein injection of CR-1 found neither death nor significant weight loss in the mice after 14 days of administration of CR-1. These results indicate that the synthesized CR-1 probe has low cytotoxicity and good biocompatibility, suggesting that it can be used for the imaging of Zn^{2+} *in vivo*.

Imaging of Zn^{2+} in Deep Tissue *in Vivo*. In order to study the feasibility of using CR-1 to image Zn^{2+} in deep tissue *in vivo*, different substances were subcutaneously injected into the mouse thigh tissue. Then, the PA signals in the mouse thigh tissue treated with different substances were measured under laser light irradiation at 710 nm and 532 nm, and the results are shown in Figure 6. The mice treated with buffer (control group) showed a negligible PA signal at 710 nm and a weak PA signal at 532 nm. This is due to the absorption of hemoglobin in the blood at the wavelength of 532

nm. Therefore, when calculating the PA_{532}/PA_{710} value, the background signal intensity of the control group should be deducted first. The mice treated with CR-1 only had a strong PA signal at 710 nm and a weak PA signal at 532 nm, with a PA_{532}/PA_{710} ratio of about 0.15. The PA signal of mice treated with 0.50 mg/kg Zn^{2+} and CR-1 at 710 nm was significantly decreased, and the PA signal at 532 nm was significantly increased, which increased the PA_{532}/PA_{710} ratio value to 0.74. Compared to mice treated with CR-1 alone, mice treated with 0.50 mg/kg Zn^{2+} and CR-1 had a PA_{532}/PA_{710} value 4.9 times higher. When Zn^{2+} was masked with TPEN, the PA_{710}/PA_{532} value was almost the same as that in mice treated with CR-1 alone, indicating that the increase of the PA_{710}/PA_{532} value was due to the presence of Zn^{2+}.

To further evaluate the potential of CR-1 for imaging of Zn^{2+} in deep-tissue *in vivo*, we simultaneously injected CR-1 and Zn^{2+} subcutaneously into mouse thigh tissue and performed PA imaging after covering on the mouse thigh surface with chicken breast tissue. As shown in Figure 7, despite the weakening of the PA signal intensity, the distribution of Zn^{2+} *in vivo* can still be visualized in the deep tissue, indicating that the synthesized CR-1 probe has the potential for imaging of Zn^{2+} in deep-tissue *in vivo*.

CONCLUSIONS

In summary, we have developed the first PA probe (CR-1) of Zn^{2+} for *in vivo* ratiometric PA imaging. This probe reacts with Zn^{2+} resulting in the blue shift of its absorption peak from 710 nm to 532 nm, which causes an increase in the PA signal at

the excitation wavelength of 532 nm, while the PA signal decreases at the excitation wavelength of 710 nm, and the ratiometric PA signal at these two wavelengths (PA_{532}/PA_{710}) exhibited a good linear relationship with the concentration of Zn^{2+}. Therefore, the CR-1 can be used to monitor the steady state changes in Zn^{2+} concentration in the tissue of living animals by ratiometric PA imaging. Furthermore, the designed probe showed a highly selective PA response to Zn^{2+} with a favourable detection limit of 170 nM. In particular, this probe displayed an extremely fast response, permitting the trapping of transient Zn^{2+} and real-time monitoring of Zn^{2+}-related biological processes. This study provides a new way for *in situ* monitoring Zn^{2+} *in vivo*, contributing to the understanding of the relationship of Zn^{2+} to various neurological diseases. More importantly, as the imaging process is reversible, it will open up new avenues for the study of the complex biochemical processes involving Zn^{2+} in deep-tissue *in vivo*.

ASSOCIATED CONTENT

Supporting Information

The Supporting Information is available free of charge on the ACS Publications website at DOI: 10.1021/acs.analchem.xxxxxxx.

Synthesis procedure of IR825; supplementary figures for ^{1}H NMR spectrum of IR825, ^{13}C NMR spectrum of IR825, MS spectrum of IR825, ^{1}H NMR spectrum of CR-1, ^{13}C NMR spectrum of CR-1, MS spectrum of CR-1, absorption spectra of CR-1 at different time, absorption spectra of CR-1

solutions at different concentrations, MS spectrum of CR-1-Zn^{2+} complex, the detection of apparent dissociation constant (K_d) for CR-1 binding to Zn^{2+}, photostability of CR-1 and ICG solution, PA images of CR-1-Zn^{2+} solution at different cycles, absorption spectra of CR-1-Zn^{2+} solutions at different time (min) under continuous wave laser irradiation, the ratio of absorption intensity (Abs_{532}/Abs_{710}) of CR-1 and CR-1-Zn^{2+} solutions under different pH, the ratio of PA intensity (PA_{532}/PA_{710}) of CR-1 and CR-1-Zn^{2+} solutions under different pH, absorption spectra of CR-1 solution in the presence of different metal ions, the ratio of absorption intensity (Abs_{532}/Abs_{710}) of CR-1 solution in the presence of different metal ions, the ratio of PA intensity (PA_{532}/PA_{710}) of CR-1 solution in the presence of different metal ions.

AUTHOR INFORMATION

Corresponding Author

*E-mail: zhaoshulin001@163.com (S.Z.) and cb.liu@siat.ac.cn (C. L.).

Notes

The authors declare no competing financial interest.

ACKNOWLEDGMENTS

This work was supported by the National Natural Science Foundations of China (Grant No. 21874030) and BAGUI Scholar Program.

REFERENCES

(1) Berg, J. M.; Shi, Y. The Galvanization of Biology: A Growing Appreciation for the Roles of Zinc, *Science* **1996**, *271*, 1081-1085.

(2) Sensi, S. L.; Paoletti, P.; Bush A. I.; Sekler, I. Zinc in the Physiology and Pathology of the CNS, *Nat. Rev. Neurosci.* **2009**, *10*, 780-791.

(3) Frederickson, C. J.; Koh, J. Y.; Bush, A. I. The Neurobiology of Zinc in Health and Disease, *Nat. Rev. Neurosci.* **2005**, *6*, 449−462.

(4) Bush, A. I.; Pettingell, W. H.; Multhaup, G.; Paradis, M. D.; Vonsattel, J. P.; Gusella, J. F.; Beyreuther, K.; Masters, C. L.; Tanzi, R. E. Rapid Induction of Alzheimer A beta Amyloid Formation by Zinc, *Science* **1994**, *265*, 1464-1467.

(5) Clavijo Jordan, M. V. C.; Lo, S.-T.; Chen, S.; Preihs, C.; Chirayil, S.; Zhang, S.; Kapur, P.; Li, W.-H.; De Leon-Rodriguez, L. M. D.; Lubag, A. J. M.; Rofsky, N. M.; Sherry, A. D. Zinc-Sensitive MRI Contrast Agent Detects Differential Release of Zn(II) Ions from the Healthy vs. Malignant Mouse Prostate, *Proc. Natl. Acad. Sci. U. S. A.* **2016**, *113*, E5464-E5471.

(6) Becker, J. S.; Zoriy, M. V.; Pickhardt, C.; Palomero-Gallagher, N.; Zilles, K. Imaging of Copper, Zinc, and Other Elements in Thin Section of Human Brain Samples (Hippocampus) by Laser Ablation Inductively Coupled Plasma Mass Spectrometry, *Anal. Chem.* **2005**, *77*, 3208-3216.

(7) Martins, A. F.; Jordan, V. C.; Bochner, F.; Chirayil, S.; Paranawithana, N.; Zhang, S.; Lo, S. T.; Wen, X.; Zhao, P.; Neeman, M.; Sherry, A. D. Imaging Insulin Secretion from Mouse Pancreas by MRI Is Improved by Use of a

Zinc-Responsive MRI Sensor with Lower Affinity for Zn^{2+} Ions, *J. Am. Chem. Soc.* **2018**, *140*, 17456−17464.

(8) Komatsu, K.; Urano, Y.; Kojima, H.; Nagano, T. Development of an Iminocoumarin-Based Zinc Sensor Suitable for Ratiometric Fluorescence Imaging of Neuronal Zinc, *J. Am. Chem. Soc.* **2007**, *129*, 13447-13454.

(9) Wang, L. V.; Hu, S. Photoacoustic Tomography: In Vivo Imaging from Organelles to Organs, *Science* **2012**, *335*, 1458-1462.

(10) Pu, K. Y.; Shuhendler, A. J.; Jokerst, J. V.; Mei, J. G.; Gambhir, S. S.; Bao, Z. N.; Rao, J. H. Semiconducting Polymer Nanoparticles as Photoacoustic Molecular Imaging Probes in Living Mice, *Nat. Nanotechnol.* **2014**, *9*, 233−239.

(11) Jathoul1, A. P.; Laufer, J.; Ogunlade, O.; Treeby, B.; Cox, B.; Zhang, E.; Johnson, P.; Pizzey, A. R.; Philip, B.; Marafioti, T.; Lythgoe, M. F.; Pedley, R. B.; Pule, M. A.; Beard, P. Deep in Vivo Photoacoustic Imaging of Mammalian Tissues Using a Tyrosinase-Based Genetic Reporter, *Nat. Photon.* **2015**, *9*, 239–246.

(12) Xie, C.; Zhen, X.; Lyu, Y.; Pu, K. Nanoparticle Regrowth Enhances Photoacoustic Signals of Semiconducting Macromolecular Probe for In Vivo Imaging, *Adv. Mater.* **2017**, *29*, 1703693.

(13) Reinhardt, C. J.; Zhou, E. Y.; Jorgensen, M. D.; Partipilo, G.; Chan, J. A Ratiometric Acoustogenic Probe for in Vivo Imaging of Endogenous Nitric Oxide, *J. Am. Chem. Soc*. **2018**, *140*, 1011−1018.

(14) Yao, J.; Kaberniuk, A. A.; Li, L.; Shcherbakova, D. M.; Zhang, R.; Wang, L.;

Li, G.; Verkhusha, V. V.; Wang, L. V. Multiscale Photoacoustic Tomography using Reversibly Switchable Bacterial Phytochrome as a Near-Infrared Photochromic Probe, *Nat. Methods* **2016**, *13*, 67–73.

(15) Wang, Y.; Hu, X.; Weng, J.; Li, J.; Fan, Q.; Zhang, Y.; Ye, D. A Photoacoustic Probe for the Imaging of Tumor Apoptosis by Caspase-Mediated Macrocyclization and Self-Assembly, *Angew. Chem*. **2019**, *131*, 4940-4944.

(16) Knox, H. J.; Hedhli, J.; Kim, T. W.; Khalili, K.; Dobrucki, L. W.; Chan, J. A Bioreducible N-Oxide-Based Probe for Photoacoustic Imaging of Hypoxia, *Nat. Commun.* **2017**, *8*, 1794.

(17) Yin, L.; Sun, H.; Zhang, H.; He, L.; Qiu, L.; Lin, J.; Xia, H.; Zhang, Y.; Ji, S.; Shi, H.; Gao, M. Quantitatively Visualizing Tumor-Related Protease Activity in Vivo Using a Ratiometric Photoacoustic Probe, *J. Am. Chem. Soc.* **2019**, *141*, 3265−3273.

(18) Roberts, S.; Seeger, M.; Jiang, Y.; Mishra, A.; Sigmund, F.; Stelzl, A.; Lauri, A.; Symvoulidis, P.; Rolbieski, H.; Preller, M.; Deán-Ben, X. L.; Razansky, D.; Orschmann, T.; Desbordes, S. C.; Vetschera, P.; Bach, T.; Ntziachristos, V.; Westmeyer, G. G. Calcium Sensor for Photoacoustic Imaging, *J. Am. Chem. Soc.* **2018**, *140*, 2718−2721.

(19) Mishra, A.; Jiang, Y.; Roberts, S.; Ntziachristos, V.; Westmeyer, G. G. Near-Infrared Photoacoustic Imaging Probe Responsive to Calcium, *Anal. Chem*. **2016**, *88*, 10785−10789.

(20) Li, H.; Zhang, P.; Smaga, L. P.; Hoffman, R. A.; Chan, J. Photoacoustic Probes

for Ratiometric Imaging of Copper(II), *J. Am. Chem. Soc.* **2015**, *137*, 15628−15631.

(21) Ikeno, T.; Hanaoka, K.; Iwaki, S.; Myochin, T.; Murayama, Y.; Ohde, H.; Komatsu, T.; Ueno, T.; Nagano, T.; Urano, Y. Design and Synthesis of an Activatable Photoacoustic Probe for Hypochlorous Acid, *Anal. Chem.* **2019**, *91*, 9086−9092.

(22) Liu, Y.; Wang, S.; Ma, Y.; Lin, J.; Wang, H. Y.; Gu, Y.; Chen, X.; Huang, P. Ratiometric Photoacoustic Molecular Imaging for Methylmercury Detection in Living Subjects, *Adv. Mater*. **2017**, *29*, 1606129.

(23) Guo, B.; Sheng, Z.; Hu, D., Liu, C.; Zheng, H.; Liu, B. Through Scalp and Skull NIR-II Photothermal Therapy of Deep Orthotopic Brain Tumors with Precise Photoacoustic Imaging Guidance, *Adv. Mater.* **2018**, *30,* 1802591.

(24) Kiyose, K.; Kojima, H.; Urano, Y.; Nagano, T. Development of a Ratiometric Fluorescent Zinc Ion Probe in Near-Infrared Region, Based on Tricarbocyanine Chromophore, *J. Am. Chem. Soc*. **2006**, 128, 6548-6549.

(25) Guo, Z.; Kim, G. H.; Yoon, J.; Shin, I. Synthesis of a Highly Zn^{2+}-Selective Cyanine-Based Probe and Its Use for Tracing Endogenous Zinc Ions in Cells and Organisms, *Nat. Protocols* **2014**, *9*, 1245-1254.

(26) Guo, Z.; Kim, G. H.; Shin, I.; Yoon, J. A Cyanine-Based Fluorescent Sensor for Detecting Endogenous Zinc Ions in Live Cells and Organisms, *Biomaterials* **2012**, *33*, 7818-7827.

(27) Gruenwedel, D. W. Multidentate Coordination Compounds. Chelating

Properties of Aliphatic Amines Containing .alpha.-Pyridyl Residues and Other Aromatic Ring Systems as Donor Groups, *Inorg. Chem.* **1968**, *7*, 495-501.

(28) Que, E. L.; Domaille, D. W.; Chang, C. J. Metals in Neurobiology: Probing Their Chemistry and Biology with Molecular Imaging, *Chem. Rev.* **2008,** *108,* 1517–1549.

(29) Leibold, N. K.; van den Hove, D. L. A.; Esquivel, G.; De Cort, K.; Goossens, L.; Strackx, E.; Buchanan, G. F.; Steinbusch, H. W. M.; Lesch, K. P.; Schruers, K. R. J. The Brain Acid–Base Homeostasis and Serotonin: A Perspective on the Use of Carbon Dioxide as Human and Rodent Experimental Model of Panic, *Prog. Neurobiol.* **2015**, *129*, 58–78.

FIGURE CAPTIONS

Scheme 1. Schematic diagram of the CR-1 reaction with Zn^{2+} (a) and its application for ratiometric PA imaging of Zn^{2+} *in vivo* (b).

Figure 1. The syntheti c route of CR-1.

Figure 2. The absorption and PA characteristics of the CR-1 reaction with Zn^{2+}. (a) UV-vis absorption spectra of CR-1 solutions (10 mM HEPES containing 10% acetonitrile, pH=7.4) with different concentrations of Zn^{2+}, inset diagram shows the change of color of the solution before and after the reaction between CR-1 and Zn^{2+}; (b) the PA signals of CR-1 solution at 710 nm and at 532 nm with different concentrations of Zn^{2+}; (c) linear relationship between the ratio of absorption intensity (Abs_{532}/Abs_{710}) of CR-1 solution and the concentration of Zn^{2+} in the range of 0-5 μM; (d) the linear relationship between the ratio of PA intensity (PA_{532}/PA_{710}) of the CR-1 solution (50 μM) and the concentration of Zn^{2+} in the range of 0-50 μM.

Figure 3. (a) The reversible change of the ratiometric absorption intensity after the addition of Zn^{2+} or TPEN in the CR-1 HEPES solution; (b) the reversible change of the ratiometric PA intensity after the addition of Zn^{2+} or TPEN in the CR-1 HEPES solution.

Figure 4. Specificity of the CR-1 towards Zn^{2+}. (a) PA imaging of the CR-1 solution (50 μM CR-1, 10 mM HEPES containing 10% acetonitrile, pH=7.4) at 710 nm and 532 nm in the presence of different metal ions; (b) the ratio of PA intensity in the CR-1 solution (50 μM) at 710 nm and 532 nm in the presence of different metal ions. The metal ions 1→18: blank, Ag^{+}， Fe^{2+}， Ca^{2+}，

Fe^{3+}, Ni^{2+}, Cd^{2+}, Cu^{2+}, Na^{+}, K^{+}, Al^{3+}, Pb^{2+}, Cr^{3+}, Mn^{2+}, Hg^{2+}, Co^{2+}, Mg^{2+}, Zn^{2+} (Zn^{2+} is 50 μM, Na^{+}, K^{+}, Ca^{2+} and Mg^{2+} is 5 mM, and other metal ions are 100 μM); (c) the ratio of absorption intensity (Abs_{532}/Abs_{710}) of the CR-1 solution (5 μM) at 710 nm and 532 nm under the coexistence of Zn^{2+} and different metal ions. The metal ions 1→18: blank, Zn^{2+}, Zn^{2+}+Al^{3+}, Zn^{2+}+Ca^{2+}, Zn^{2+}+Fe^{3+}, Zn^{2+}+Cd^{2+}, Zn^{2+}+Co^{2+}, Zn^{2+}+Cr^{3+}, Zn^{2+}+Hg^{2+}, Zn^{2+}+Fe^{2+}, Zn^{2+}+K^{+}, Zn^{2+}+Mg^{2+}, Zn^{2+}+Cu^{2+}, Zn^{2+}+Mn^{2+}, Zn^{2+}+Na^{+}, Zn^{2+}+Ni^{2+}, Zn^{2+}+Pb^{2+}, Zn^{2+}+Ag^{+} (5 μM each).

Figure 5. (a) Survival rate of 22Rv1 cells after 24 h incubation with different concentrations of CR-1. (b) Body weight change of the mice during 14 days following the intravenous injection of PBS (control group) and CR-1 (3 mg/kg) into the tail vein of the mice.

Figure 6. The imaging of Zn^{2+} in thigh tissue of living mouse. (a) *In vivo* ultrasound (US) and PA imaging of mice treated with buffer (control), CR-1, 0.25 mg/kg Zn^{2+}+CR-1, 0.50 mg/kg Zn^{2+}+CR-1, Zn^{2+}+TPEN+CR-1 at 710 and 532 nm; (b) PA signal intensity of mice treated with different substances at 710 and 532 nm; (c) changes in the PA signal intensity ratio (PA_{532}/PA_{710}) of mice treated with different substances at 710 and 532 nm, with an inline image of the PA ratio. $^{**}p < 0.01$, the data were expressed as mean ± standard deviation (n=3).

Figure 7. The PA imaging of Zn^{2+} in deep tissue of living animals. (a) PA imaging at 532 nm and 710 nm, and ultrasound (US) imaging of mice treated with Zn^{2+} and CR-1 after the mouse thigh surface was covered with chicken breast tissue; (b) the PA signal strength corresponding to that in (a).

Scheme 1

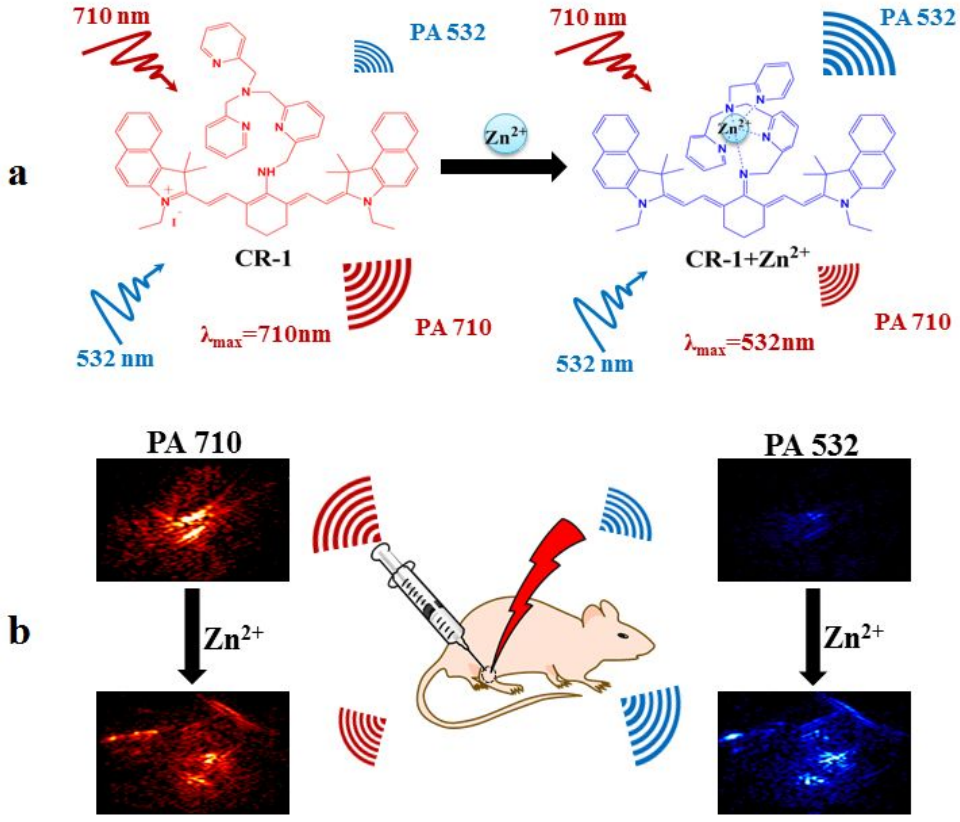
a
710 nm
PA 532
CR-1
532 nm
λmax=710nm
PA 710
Zn2+
710 nm
PA 532
CR-1+Zn2+
532 nm
λmax=532nm
PA 710
b
PA 710
Zn2+
PA 532
Zn2+

Figure 1

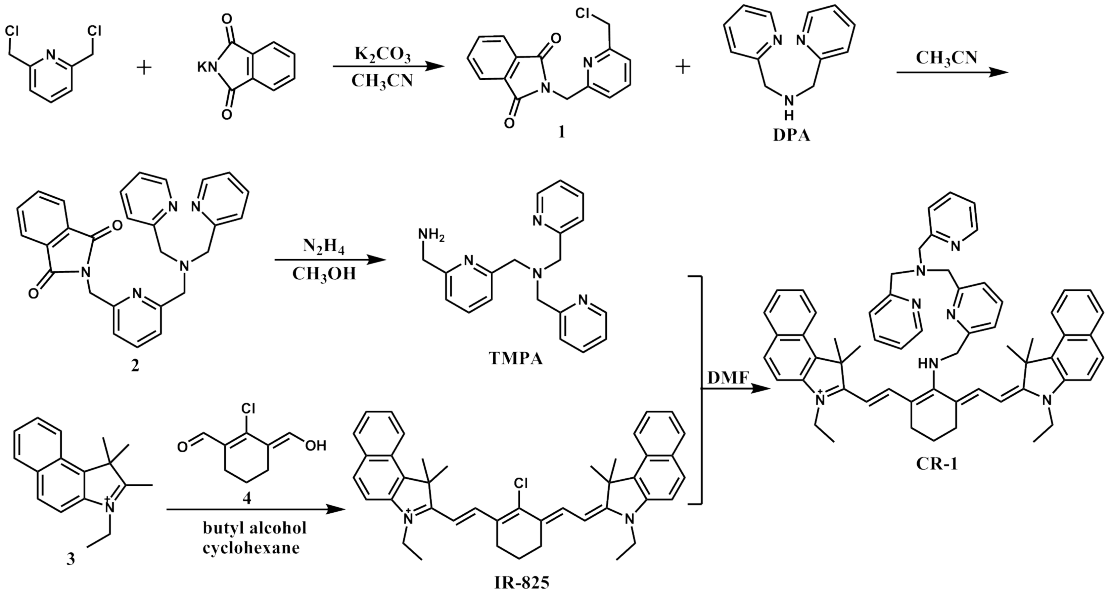
K2CO3
CH3CN
1
DPA
CH3CN
2
N2H4
CH3OH
TMPA
DMF
CR-1
3
4
butyl alcohol
cyclohexane
IR-825

Figure 2

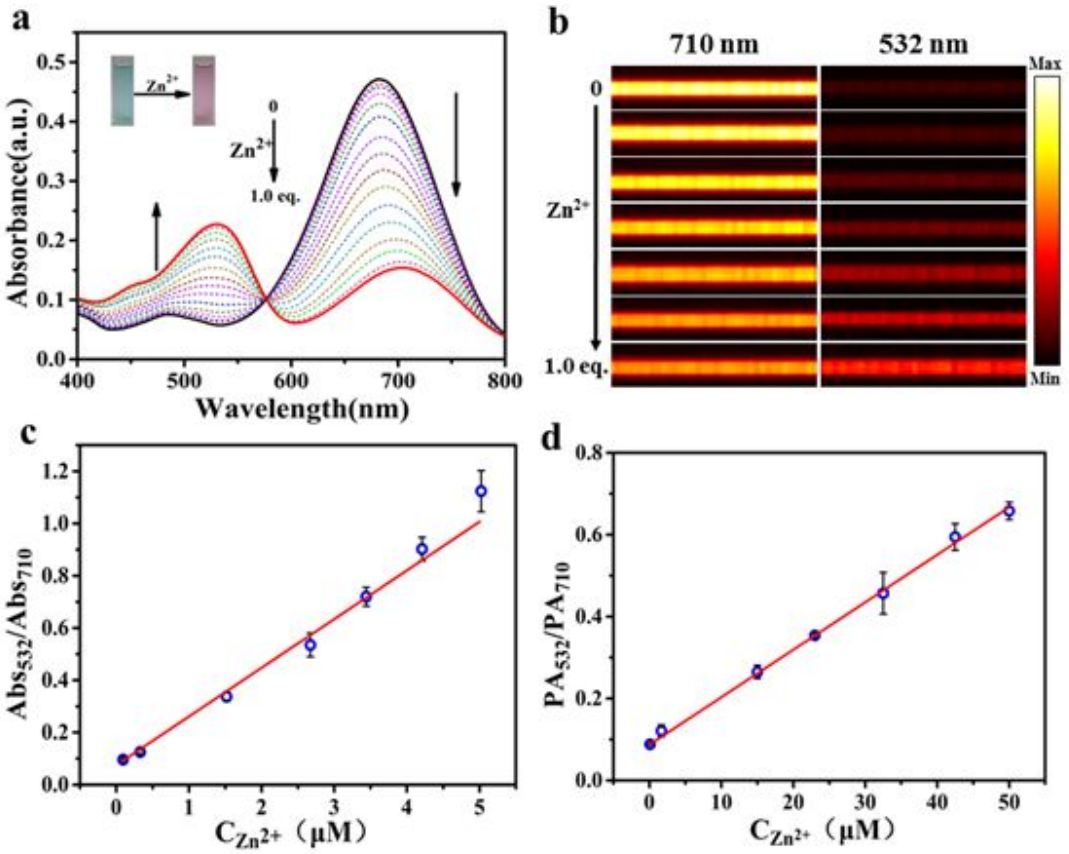
a
Absorbance(a.u.)
Wavelength(nm)
Zn2+
0
1.0 eq.
b
710 nm
532 nm
Max
Min
c
Abs532/Abs710
CZn2+ (μM)
d
PA532/PA710
CZn2+ (μM)

Figure 3

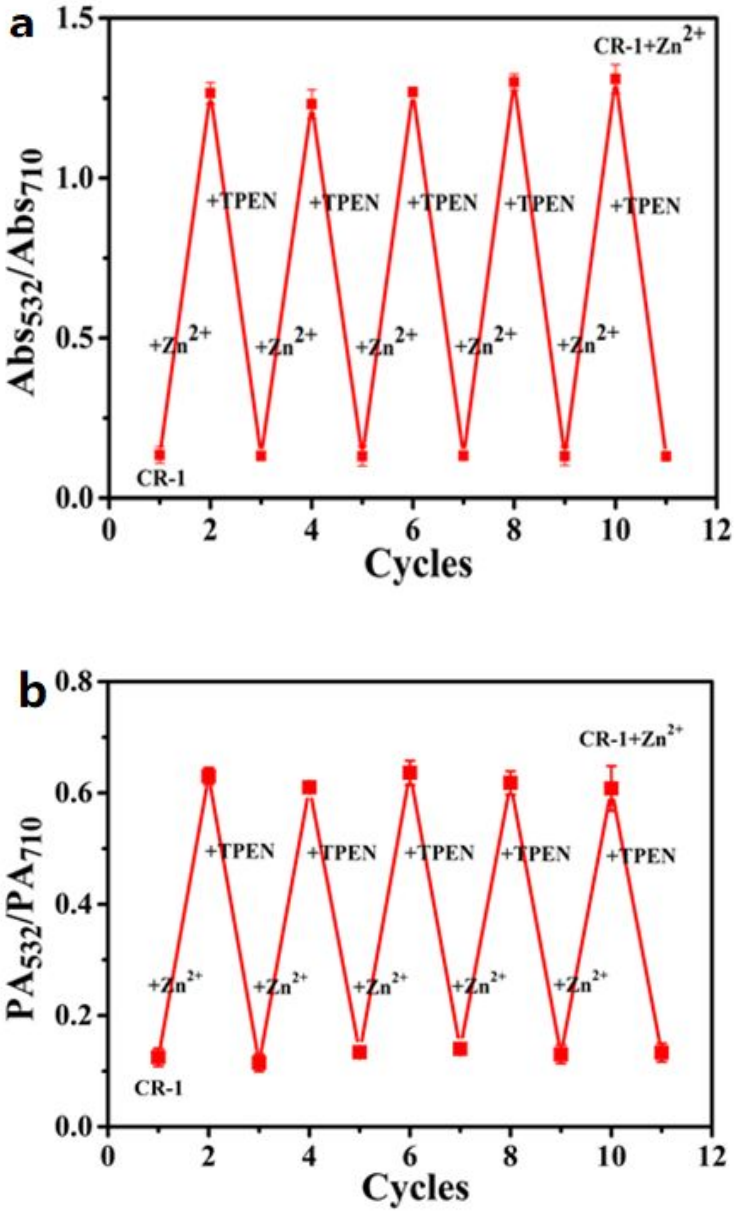

Figure 4

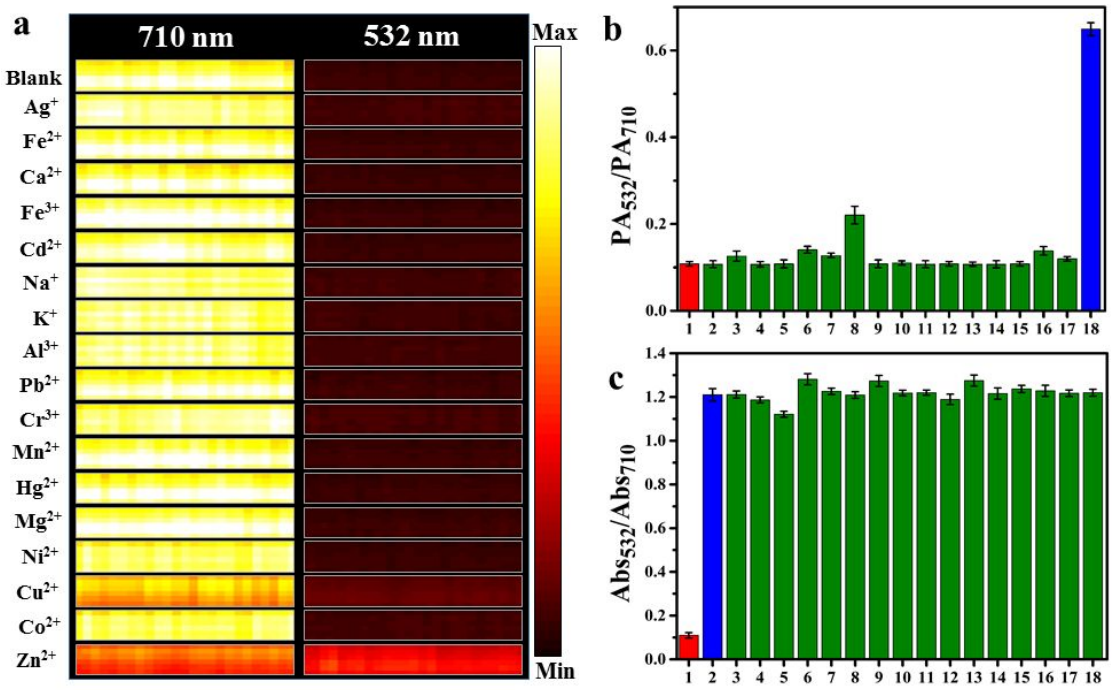
a
710 nm
532 nm
Max
Min
Blank
Ag+
Fe2+
Ca2+
Fe3+
Cd2+
Na+
K+
Al3+
Pb2+
Cr3+
Mn2+
Hg2+
Mg2+
Ni2+
Cu2+
Co2+
Zn2+
b
PA532/PA710
c
Abs532/Abs710
1 2 3 4 5 6 7 8 9 10 11 12 13 14 15 16 17 18

Figure 5

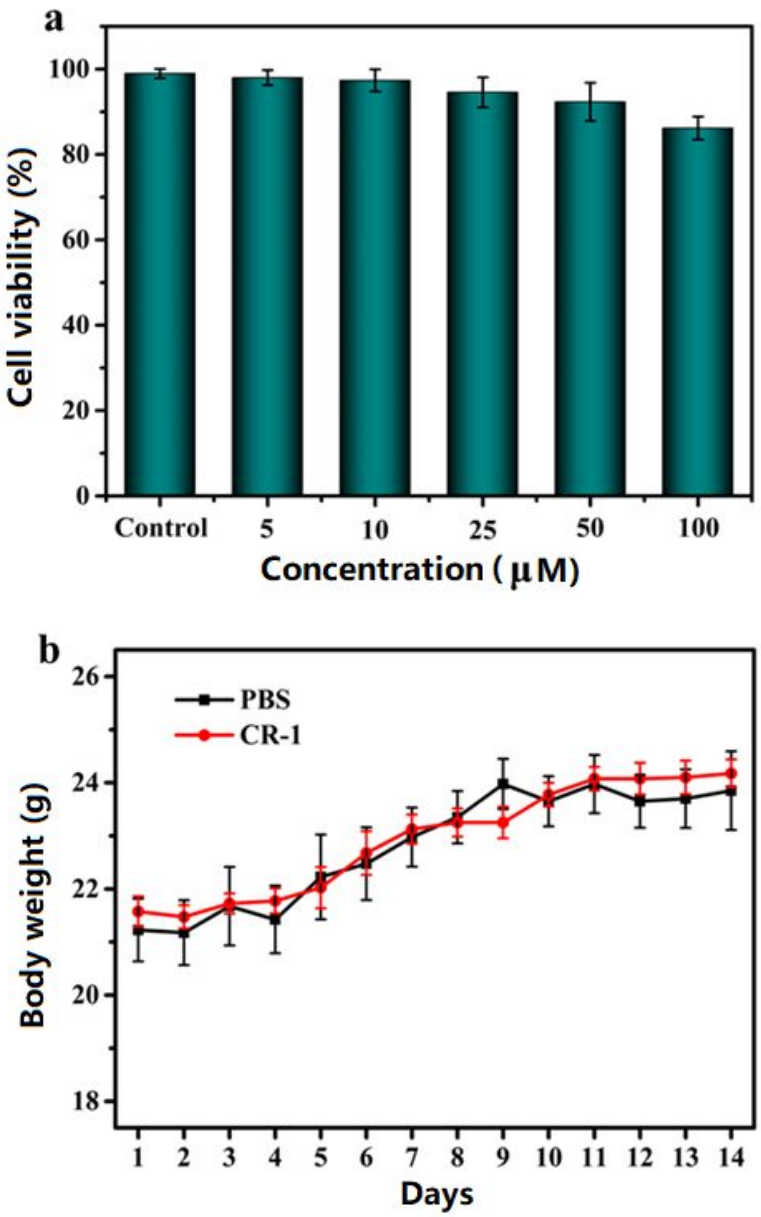
a
Cell viability (%)
0
20
40
60
80
100
Control
5
10
25
50
100
Concentration (μM)
b
Body weight (g)
18
20
22
24
26
PBS
CR-1
1
2
3
4
5
6
7
8
9
10
11
12
13
14
Days

Figure 6

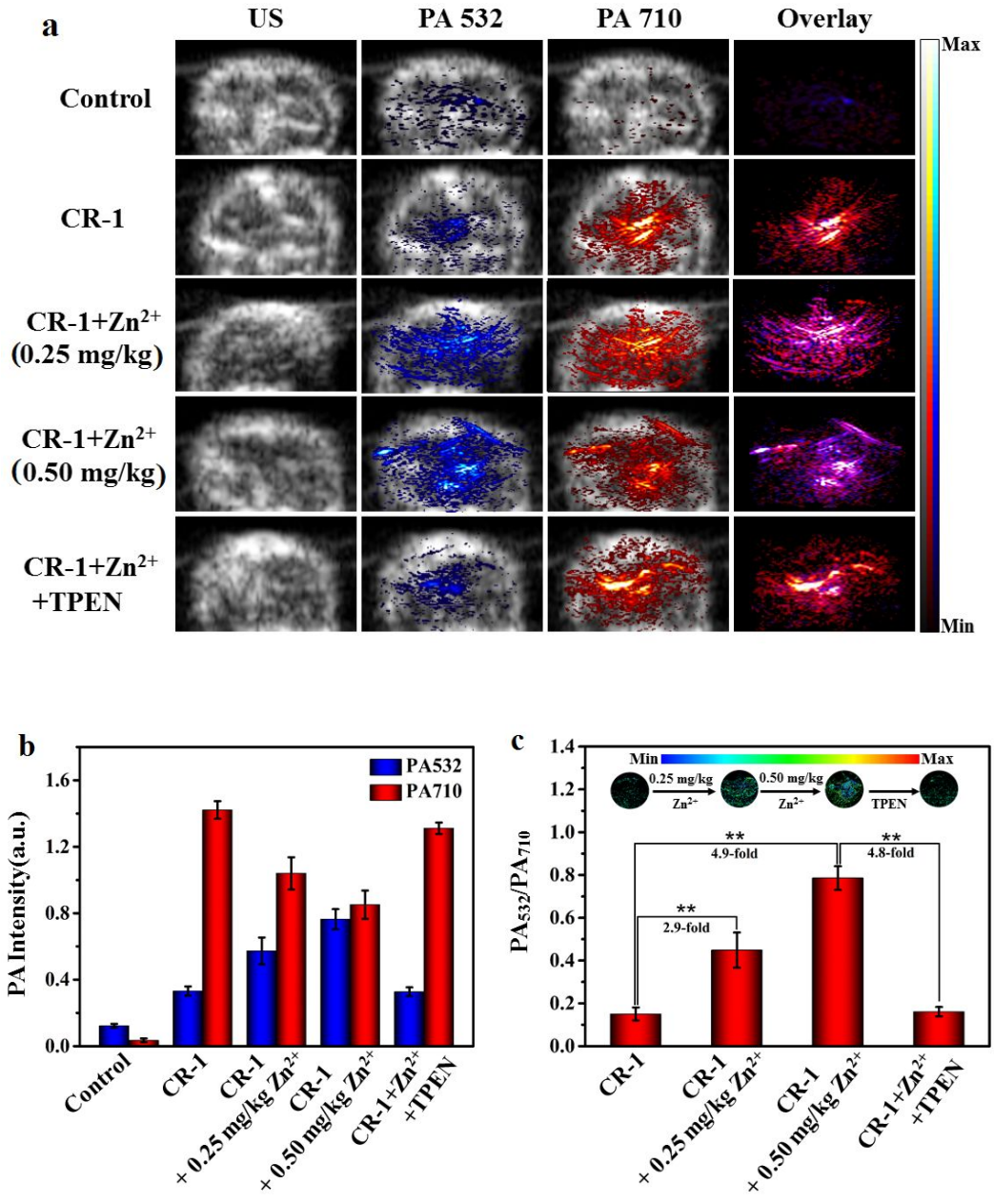
a
US
PA 532
PA 710
Overlay
Max
Min
Control
CR-1
CR-1+Zn2+ (0.25 mg/kg)
CR-1+Zn2+ (0.50 mg/kg)
CR-1+Zn2+ +TPEN
b
PA Intensity(a.u.)
PA532
PA710
Control
CR-1
CR-1 + 0.25 mg/kg Zn2+
CR-1 + 0.50 mg/kg Zn2+
CR-1+Zn2+ +TPEN
c
PA532/PA710
Min
Max
0.25 mg/kg Zn2+
0.50 mg/kg Zn2+
TPEN
**
4.9-fold
**
4.8-fold
**
2.9-fold

Figure 7

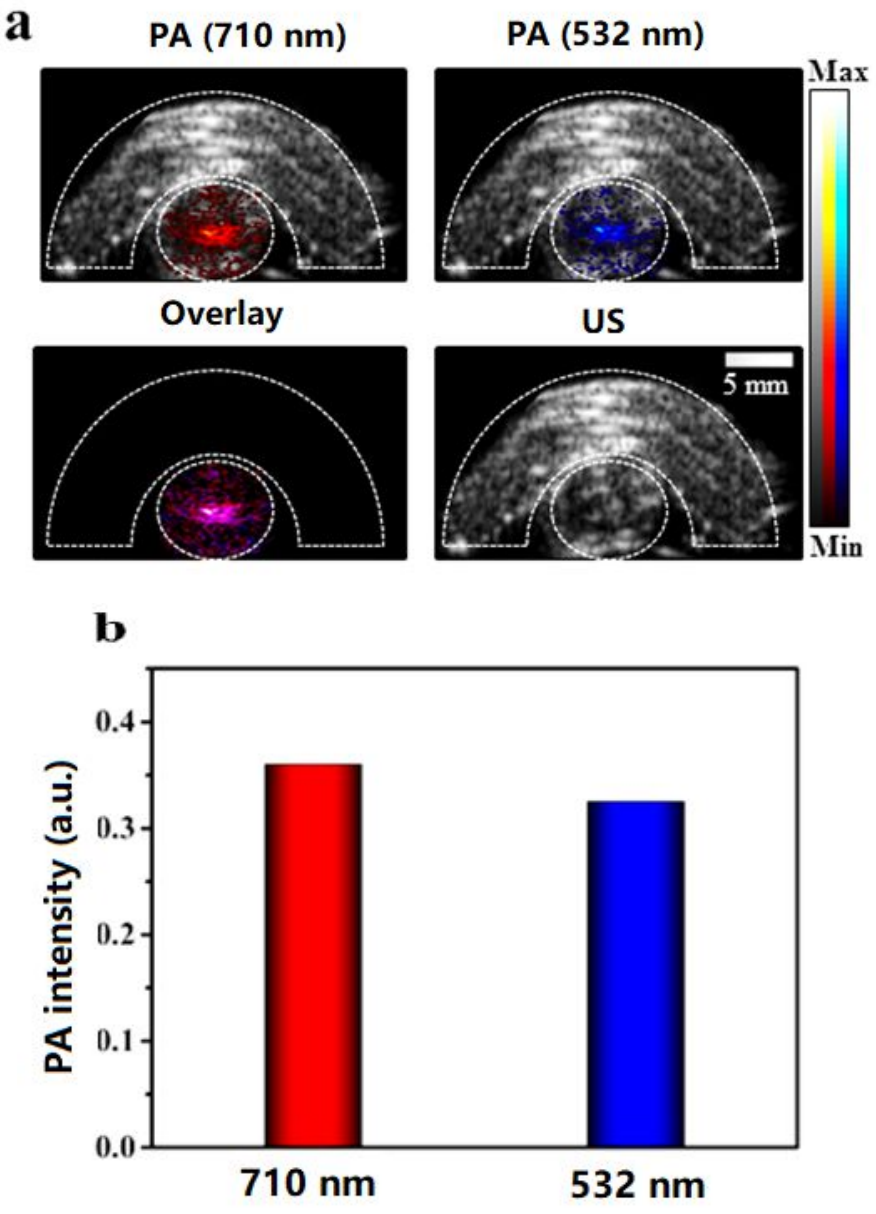
a
PA (710 nm)
PA (532 nm)
Max
Min
Overlay
US
5 mm
b
PA intensity (a.u.)
0.0
0.1
0.2
0.3
0.4
710 nm
532 nm

For TOC only